14th IEA Heat Pump Conference
15-18 May 2023, Chicago, Illinois

Numerical performance assessment of heat pumps in Rankine-based Carnot battery systems for grid balancing services

Robin Tassenoy[a,*] Jari De Craecker[a], , Katarina Simić [a], Toon Demeester[a], Michel De Paepe[a,b], Steven Lecompte[a,b]

[a]Ghent University, Sint-Pietersnieuwstraat 41, Ghent 9000, Belgium
[b]FlandersMake@UGent – Core lab EEDT-MP, Gaston Geenslaan 8, Heverlee 3001, Belgium

Abstract

Due to the increasing share of renewable sources in the energy mix, large-scale energy storage systems are becoming essential to ensure secure and stable energy supply. Carnot batteries, a combination of a power-to-heat, a thermal storage and a heat-to-power system, could provide a possible solution. Heat pump systems have been considered as the power-to-heat technology for Carnot batteries. However, it is not clear which grid services these heat pumps could deliver. To answer this question, a 1 MW vapour compression heat pump, suitable for integration in a Carnot battery, was modelled in Modelica. Quasi-steady state operation of compressor and expansion valve was considered, while dynamic finite volume models were used for the heat exchangers. Behavior of the sensible storage tanks was assumed ideal and quasi-steady boundary conditions were imposed. Furthermore, a control strategy driven by the requirements of the electrical grid was proposed. The dynamic model simulates and evaluates the heat pump's response to the qualification test profiles for grid balancing services. It was found that the heat pump can deliver a symmetric capacity of 125 kW for primary reserve while maintaining a correct delivery temperature to the thermal storage system. In addition, the system qualifies for delivering a capacity of 250 kW for secondary and tertiary reserve. These results indicate that the delivery of grid balancing services could be another revenue stream to increase the financial feasibility of Carnot battery systems and it is thus worthwhile to investigate its potential financial benefits.

Selection and/or peer-review under the responsibility of the organizers of the 14th IEA Heat Pump Conference 2023.

Keywords: Carnot battery; Rankine-based heat pump; grid balancing services; FCR; aFRR; mFRR

1. Introduction

1.1. Carnot batteries

The share of renewables in the worldwide energy generation is continuously increasing, peaking at 23.2% in 2019. This increase was even steeper in member states of the European Union, where renewable electricity production accounted for 33.2% [1]. This large deployment of variable renewable energy sources (RES) challenges the stability of the electrical grid due to their intermittent nature. Energy storage can address these problems by power and voltage smoothing, energy management, frequency regulation, peak shaving, load leveling, seasonal storage and standby generation during a fault [2]. Therefore, energy storage is considered one of the main drivers to provide the flexibility needed to completely decarbonize the electricity grid [3].

Carnot batteries are an emerging large-scale electrical energy storage (EES) concept that may provide additional flexibility to the grid. The concept involves three steps. First, electrical energy is converted into heat using a heat pump or joule heater after which the heat is stored in the second step.

* Corresponding author. Tel.: +32 9 264 33 59 .
E-mail address: Robin.Tassenoy@UGent.be .

Finally, heat engine technology is used to convert the heat back to electricity when needed. One of the Carnot battery's subsets is pumped thermal energy storage (PTES), in which an electrically driven heat pump is used to deliver heat to a hot store and/or extract heat from a cold store [4]. The majority of studies currently available have focused on the steady-state analysis and optimization of the storage concept and the obtainable round-trip efficiencies [5]. More recently, the techno-economic optimization of PTES have gained interest as well [6, 7]. Vecchi et al. [7] collected and compared the techno-economic performance data of different Carnot battery systems in literature. Moreover, they discussed the applications of Carnot batteries at energy system scale and the most recent commercial developments in Carnot battery technologies. Their literature review reveals that Carnot batteries have been considered mainly for load-shifting and arbitraging services. The authors concluded that these services alone may not be sufficient to recover the investment cost of the technology. The importance of a portfolio of grid services to provide different revenue streams is thus highlighted.

1.2. Grid balancing services

Within the portfolio of grid services, providing grid flexibility is highly promising as the need intensifies due to the large deployment of variable RES [8]. Grid flexibility is usually defined as the possibility of modifying generation and/or consumption patterns in reaction to an external signal (e.g. price) to contribute to the power system stability in a cost-effective manner. At the transmission grid level, flexibility is linked to grid balancing services offered to transmission system operators (TSOs) [9]. These services match the instantaneous electricity production and demand, which is essential to ensure stable grid operation. According to their time scale, three balancing products can be distinguished: primary or frequency containment reserve (FCR), secondary or automatically activated frequency restoration reserve (aFRR) and tertiary or manually activated frequency restoration reserve (mFRR). The FCR stabilizes the frequency deviation on the European grid at a stationary value, after which the aFRR and mFRR restore the frequency to its original value [10]. An overview of the main service characteristics is presented in Table 1.

Table 1. Characteristics of balancing services in the European electricity grid.

Balancing service	Direction	Full activation time	Min. delivery time	Min. bid size	Ref.
FCR	symmetric	30 s	15 min	1 MW	[11]
aFRR	up / down	7.5 min (to 5 min)	15 min	1 MW	[12]
mFRR	up / down	15 min	15 min	1 MW	[13]

1.3. Dynamic modelling of PTES and large-scale heat pumps with respect to grid balancing services

From the discussion above, it is clear that PTES-dynamics are essential for the delivery of grid balancing services. However, there is a lack of research on these dynamic characteristics which makes it difficult to predict, regulate and optimize the performance of PTES in actual operation processes [14].

This knowledge gap has partially been addressed for Brayton-based PTES recently [14, 15]. Lu et al. [14] constructed a dynamic simulation model of a PTES based on the closed Brayton-cycle with a nominal charging- and discharging power of 2.27 and 1.49 MW, respectively. The model was used to optimize the control strategy and dynamic performance of the system during the start-up process. It was found that the rotational speed increase rate had a negligible effect on the system startup time for the charging process but affected the start-up time of the discharging process significantly. Moreover, high rotational speed increase rates caused fluctuation and overshoot in the rotational speed. Depending on the control parameters, start-up to full load took 50 min in charging mode and 15 min in discharging mode. While the start-up was discussed, the system's reaction to disturbances of electrical power input in nominal operation was not studied. This topic was addressed by Yang et al. [15] for a 5 MW Brayton-heat pump in a PTES-system. Next to a study of the step response to the system control parameters, a closed loop inventory control strategy was proposed to ensure correct storage temperatures and high efficiency even at part-load. Although control of the system to maintain a desired power uptake, as needed for delivery of grid balancing services, was not discussed, the authors showed the system's capability to maintain correct charging conditions for the storage system despite reduced electrical power input.

To the best of the authors' knowledge, no study on the dynamics and control of a full Rankine-based PTES-system or of a heat pump cycle to be implemented in a PTES-system is currently available. Stand-alone large-scale Rankine-based heat pumps are currently mainly used in district heating applications and are thus not

optimized to react quickly to the needs of the electrical grid. Consequently, providing grid flexibility using large-scale Rankine-based heat pumps is not well understood [16]. Meesenburg et al. [17] were probably first to address this issue. A detailed numerical system model of a two-stage ammonia heat pump used in district heating applications was developed and calibrated based on experimental data. Rooted on this model, they assessed how fast large-scale heat pumps can adapt their load according to grid requirements, the dynamic effects during fast-regulation and the limitations of currently implemented units with regard to fast-regulation. It was found that after optimization of the control structure, the heat pump power could be regulated from 250 kW to 175 kW in 54 s and from 250 kW to 100 kW in 99 s without the risk of condensation in the suction line.

1.4. Scope of this study

As illustrated by the discussion above, the dynamic response and control of PTES driven by requirements of the electrical grid is a clear gap in literature. For Brayton-based PTES, the dynamic response to power disturbances has been addressed. Nevertheless, control of the system to follow a desired electrical consumption or production profile as required for grid balancing has not yet been studied. For Rankine-based PTES, no study discussing the dynamic response of the complete system has been found. In fact, only one study addressing this subject for a stand-alone large-scale heat pump has been identified. However, this study focused on an existing heat pump for district heating, which means the topology, working temperatures and temperature requirements of the heat transfer fluid to the thermal storage were less strict compared to PTES-applications. As such, it remains unclear whether PTES is capable of delivering grid balancing services. This study aims to make a first step towards answering this question by focusing on the heat pump component of Rankine-based PTES. A dynamic model of a 1 MW Rankine-based heat pump cycle suitable for implementation in a PTES was constructed. Then, a suitable control strategy to follow the desired power uptake was developed, while maintaining correct storage temperatures. Finally, the controlled system was validated against pre-qualification tests of the European grid to assess its technical potential to deliver grid balancing services.

The system description, nominal operating conditions, sizing and dynamic modelling of the components and test conditions, are described in Section 2. The modelling results are shown and discussed in Section 3. First, the Modelica model is validated by a steady-state comparison to the Python cycle calculation. Then, the maximum capacity is determined and the qualification tests for mFRR, aFRR and FCR are successively discussed before a conclusion is formulated in Section 4.

2. Methodology

2.1. Carnot-battery lay-out and heat pump boundary conditions

This work focusses on the dynamic modelling of a vapour compression heat pump to be implemented in a Carnot battery. These PTES-systems usually consists of a heat pump, a thermal storage system and a thermal engine, as shown in Figure 1.

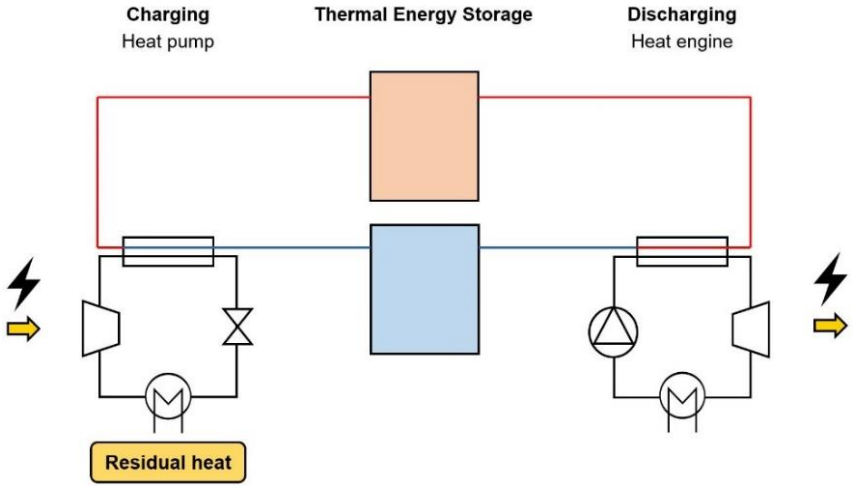

Fig. 1. Schematic representation of a Rankine-based, thermally integrated Carnot battery.

Rankine-based PTES typically takes advantage of a low-grade heat source to boost the electric round-trip efficiency of the system [18]. Apart from low grade geothermal heat and solar thermal energy, heat sources of suitable thermal capacity and temperature level can be found mostly in the industrial sector. Marina et al. [19] inventoried these industrial residual heat sources suitable for heat pump integration. The amount of residual heat available reduces with increasing heat temperature. Balancing the heat availability and efficiency improvement of the PTES, a residual heat source of 65°C was adopted in this study.

Sensible liquid heat storage is often applied as it is reliable, mature and cost-efficient. A two-tank configuration guarantees almost constant charge and discharge profiles and was therefore selected instead of a single tank solution, despite the cost of doubling the storage volume [18, 20]. Pressurized water tanks were opted for as they are cheap, have low environmental impact and are suitable for the temperature range of interest [5, 21]. As typical temperature lifts of heat pumps reported in literature range from 40 to 80 °C [22, 23], the tank temperatures were chosen to fit within this lift range. The temperature of the hot tank was chosen as 125 °C, while a cold tank temperature of 95 °C was assumed.

A basic heat pump cycle was chosen in this work. It has four main components: an evaporator, a compressor, a condenser and an expansion valve (see Fig. 1). In literature, more advanced cycles have been proposed [20, 22, 24]. Although these systems have higher coefficients of performance, the additional components increase the thermal inertia of the system and are thus expected to slow down the system's dynamic response. Therefore, the most basic system was assessed first. If this topology proves to be suitable to deliver grid balancing services, more complex topologies can be addressed in future work.

2.2. Nominal operating conditions and refrigerant selection

Once the temperature range of the heat pump had been fixed, the working fluid was selected. Based on different studies, R-1233zd(E) was selected because of its good thermodynamic performance in the intended operating range and low global warming and ozone depletion potential compared to refrigerants commonly applied [25, 26].

The steady-state operating conditions were calculated using a Python toolbox to model basic and advanced heat pump concepts [27]. Fluid property data were imported from REFPROP 10.0 [28]. Based on these estimates, more detailed component selection and modelling were performed, as discussed in Section 2.3. An overview of the modelling assumptions and resulting nominal conditions is given in Table 2.

Table 2. Nominal operating conditions: modelling assumptions and results.

Assumed parameter	Value	Unit	Output parameter	Value	Unit
$T_{water,source,in}$	65	°C	$P_{evaporator}$	2.93	bar
$T_{water,sink,in}$	95	°C	$P_{condenser}$	19.08	bar
$T_{refrigerant,sat,evaporator}$	50	°C	PR	6.5	-
$T_{refrigerant,sat,condenser}$	130	°C	$\dot{m}_{water,source}$	43.4	kg/s
$\Delta T_{superheat}$	9	°C	$\dot{m}_{water,sink}$	20.7	kg/s
$\Delta T_{subcooling}$	4	°C	$\dot{m}_{refrigerant}$	22.4	kg/s
$\dot{Q}_{condenser}$	2.8	MW	$\dot{Q}_{evaporator}$	1.81	MW
$PP_{evaporator}$	5	°C	$\dot{Q}_{condenser}$	2.80	MW
$PP_{condenser}$	5	°C	$P_{el,compressor}$	0.99	MW
$\eta_{is,compressor}$	0.8	-			
Refrigerant	R-1233zd(E)	-			

2.3. Component selection and modelling

A dynamic heat pump model was built in the object-oriented modelling language Modelica [29], using the simulation software Dymola 2022 [30] and the TIL-library [31]. The component models of this library were used, and extended when necessary. The piping pressure losses on the low and high pressure side were merged in one common pressure loss model at each pressure side to ensure right inlet and outlet pressure for the compressor. Fluid properties were calculated using the REFPROP-database [28]. In the following subsections, the component selection and assumptions made for their modelling are briefly discussed.

2.3.1. Heat exchangers

Plate heat exchangers (PHE) were selected for both the evaporator and condenser because they are relatively cheap, compact and have a modular design [20, 32]. Funke [33] produces gasketed PHE with capacities up to 30 MW and volume flow rates up to 4500 m³/h. SWEP [34] manufactures smaller capacity heat exchangers, but provides an intuitive sizing tool for high-level sizing of the heat exchangers. Based on this tool, five VH500TM PHEs and two B500TM PHEs were selected as evaporator and condenser respectively. The PHEs were modelled using the finite volume (FV) model available in the TIL-library [31], assuming countercurrent flow. Instead of modelling five separate evaporators, only one PHE model was used with the total amount of plates. The dimensions of one plate were based on the actual heat exchanger. A similar approach was implemented for the condenser. The suitability of FV-models for dynamic simulation of evaporators and condensers has extensively been demonstrated [32]. Moreover, the PHE model from the TIL-library used in this study has been successfully used to simulate a two-stage ammonia heat pump with a thermal capacity of 800 kW [17]. The authors validated the model to experimental measurements of an actual heat pump with shell-and-plate heat exchangers under identical operating conditions. Despite the different heat exchanger type, the alternative heat exchanger model accurately represented the general trends of the heat pump behavior during load change and could thus be used to assess to study the system control. In the current study, not all model parameters were made available by the PHE manufacturer. Therefore, the values reported by Meesenburg et al. [17] were used initially and adapted so that the heat exchanger mass, volume and heat exchanger area matched the values proposed by the SWEP-software [35]. Consequently, the inertia of the modelled heat exchangers is representative for the selected components. On the refrigerant side, following heat transfer correlations were applied: Shah Chen [36] for evaporation, Chen [36] for condensation and Gnielinski Dittus Boelter for single-phase flow [37]. Heat transfer at the water side was modelled by the VDI Plate alpha correlation [38]. Finally, all pressure drops in the heat exchangers were assumed proportional to quadratic mass flow [17].

2.3.2. Compressor model

A screw compressor or centrifugal compressor would be most suitable for the nominal flow rate and pressure ratio [39]. However, performance data at variable rotational speeds was not found for both. Therefore, performance maps for an axial compressor, suitable for higher flow rates, were retrieved from the GasTurb performance map collection [40] and scaled to the intended nominal conditions. An important remark to make is that the performance map used is representative for gas compressors, while in the current study a refrigerant was used. Nevertheless, the performance map of the gas compressor allowed to construct a performance map-based compressor model. The reported isentropic efficiencies range from 65 to 87 % depending on the operating conditions, which corresponds with common assumptions in performance studies for Carnot batteries. Therefore, this assumption was considered acceptable for the current purpose and the results can be updated when more suitable performance data becomes available. Immediate response of the compressor was assumed [17, 41, 42].

2.3.3. Valve model

The valve model was retrieved from the TIL-library [31]. The operating point was adapted by regulating the effective flow area of the valve.

2.3.4. Other components

The sensible storage was not modelled in detail. Instead, it was assumed that the tank was perfectly stratified and the water temperature at the inlet of the condenser stayed constant. A boundary model was used to impose a constant pressure and temperature, while the mass flow could be regulated.

2.4. Controller design

The control system should make sure the heat pump responds quickly to a desired power uptake, while maintaining correct storage temperatures and maximizing operational efficiency. Therefore, three inputs were controlled using PI-controllers: the compressor rotational speed, the valve through-flow area and the water mass flow rate in the condenser. Variable speed control of the compressor is an effective way to modulate the power uptake. A PI-controller compared the desired power consumption with the effective one and changed the rotational speed accordingly. As the operating point is determined by the intersection of the compressor- and valve characteristic, the effective through-flow area of the valve was varied to acquire the mass flow corresponding with the maximal efficiency of the compressor for a given pressure ratio. The value of the

refrigerant mass flow was calculated based on a fourth degree polynomial derived from the efficiency map of the compressor optimizing the relation between pressure ratio and mass flow rate. Finally, the water mass flow rate in the evaporator was adapted by a PI-controller to maintain a hot storage temperature of 125°C. All PI-constants were determined by analyzing the corresponding system step response using a dedicated online toolbox [43]. The resulting PI-constants are summarized in Table 3.

Table 3. PI-control parameters.

Controller	k [-]	T_i [s]
Compressor	2.412325169e-7	0.739237526841722
Valve	4.034429164e-6	0.162573741351303
Water mass flow	5	7

2.5. Test conditions for ancillary services

The Belgian TSO Elia provides prequalification tests for all balancing services discussed in Table 1. All tests follow the same approach. A power profile that represents the most extreme testing situation is provided. The service is then evaluated in terms of the full activation time (FAT), the maximum power delivery, the duration of the service and the deviation of the power. The delivery of FCR is always symmetric and the capacity should react linearly to the frequency deviation of the grid. aFRR and mFRR on the other hand can deliver up- or down regulation separately, or do both. It should be noted that Elia sets a minimum capacity bid for aFRR and mFRR at 1MW, but it is allowed to split this capacity over multiple assets. The main criterium is that the requested power uptake or production (within predefined accuracy) is reached within the prescribed maximum activation time. In this study, the combination of up-and down regulation was not tested as it follows from the separate tests. The pre-regulation tests also aim at verifying that the service can be delivered for a sufficiently long time. For Carnot batteries, this duration is closely related with the capacity and state-of-charge of the thermal storage system. Here, focus was given to the reaction time and it was assumed the TES was sized adequately, fulfilling the duration requirement.

3. Results and discussion

3.1. Steady-state model validation

A direct validation of the separate component models to experimental data is not possible, as this data is not available. Instead, the component sizing and modelling are partially validated by comparison of the steady-state results to the steady-state Python calculation. The dynamic model (and implemented control) are tested by simulating the steady-state system response to constant controller setpoints. An overview of the assumed boundary conditions, controller setpoints and corresponding simulation results is given in Table 4. The simulation results show good correspondence with the steady-state cycle calculations in Table 2. The deviation can be explained by the model strategy. While the thermodynamic states are fixed directly in the Python model, they follow from the physical component characteristics and choice of controlled parameters in the Modelica model. A one-on-one match is thus not to be expected. Nevertheless, the good correspondence between results indicates proper sizing and modelling of the different components. Moreover, the controllers reach the desired setpoint illustrating the effectiveness of the implemented control method.

Table 4: Steady-state model validation - boundary conditions and simulation results.

Assumed parameter	Value	Unit	Output variable	Value	Unit
$T_{water,source,in}$	65	°C	$T_{water,sink,out}$	125	°C
$T_{water,sink,in}$	95	°C	$P_{el,compressor}$	1.00	MW
$T_{water,sink,out,set}$	125	°C	$P_{evaporator}$	2.98	bar
$\dot{m}_{water,source}$	43.4	kg/s	$P_{condenser}$	19.52	bar
$P_{el,compressor,set}$	1	MW	PR	6.54	-
Refrigerant	R-1233zd(E)	-	$\dot{m}_{water,sink}$	19.41	kg/s
			$\dot{m}_{refrigerant}$	23.05	kg/s

$\dot{Q}_{evaporator}$	1.48	MW
$\dot{Q}_{condenser}$	2.46	MW
$\Delta T_{superheat}$	12.68	°C
$\Delta T_{subcooling}$	0	°C
$PP_{evaporator}$	3.1	°C
$PP_{condenser}$	8.096	°C
$\eta_{is,compressor}$	0.86	-

3.2. Maximum power regulation

To assess the possibility of delivering grid balancing services, the maximum capacity available should be determined first. The minimum part-load capacity the system can run at is determined by:

- The minimum rotational speed of the compressor, which is 50% of the nominal speed according to the performance map.
- Condensation of the refrigerant at the inlet or outlet of the compressor due to insufficient superheating.
- The condenser temperature, as the heat pump may not be able to sustain a water outlet temperature of 125°C to the storage tank.

In order to test which condition limits the part-load capacity of the system, the compressor power setpoint was gradually reduced. This was done sufficiently slow so that all operating points could be considered steady-state and the operating range was not determined by transient responses. The superheating at the outlet of the compressor became insufficient first, at a compressor power uptake of 750 kW. The compressor power can thus be modulated between 750 and 1000 kW. The potential capacity for aFRR and mFRR is hence 250 kW. As FCR should always be delivered symmetrically, the potential power band for FCR is limited to 125 kW around a nominal operating point of 875 kW.

3.3. Tertiary reserve

The Carnot battery should fulfill two requirements in order to qualify for mFRR: the system should have a sufficiently low response time and should be able to maintain the correct charging temperatures to the TES.

The mFRR has a maximum FAT of 15 min, implying that the full offered capacity should be activated within 15 min. In Figure 2, the step response of the heat pump system to a step change in compressor power setpoint in the downward- and upward direction is shown. As summarized in Table 5, the FAT of the heat pump is well below the limit of 15 minutes. The response time found is significantly shorter than the minimal regulation time of 54 s obtained by Meesenburg et al. [17], who made similar modelling assumptions. This difference can be attributed to the more complex system lay-out. The one-stage heat pump reacts significantly quicker than a two-stage variant because of its lower system inertia and omitted control of the intermediate pressure level. Yang et al. [15] studied the dynamic response of a 5 MW Brayton-based heat pump integrated in a Carnot battery and found a response time of 14.28 s for a 250 kW downward ramp. The response times found for the 1MW Rankine-heat pump are thus lower, but have a similar order of magnitude for the same mFRR capacity delivered.

Table 5. FAT of a 1 MW heat pump system in downward and upward direction.

Full activation time [s]	Downward step	Upward step
Within 1% deviation	4.1	3.7
Within 0.1 %	6.4	7.3

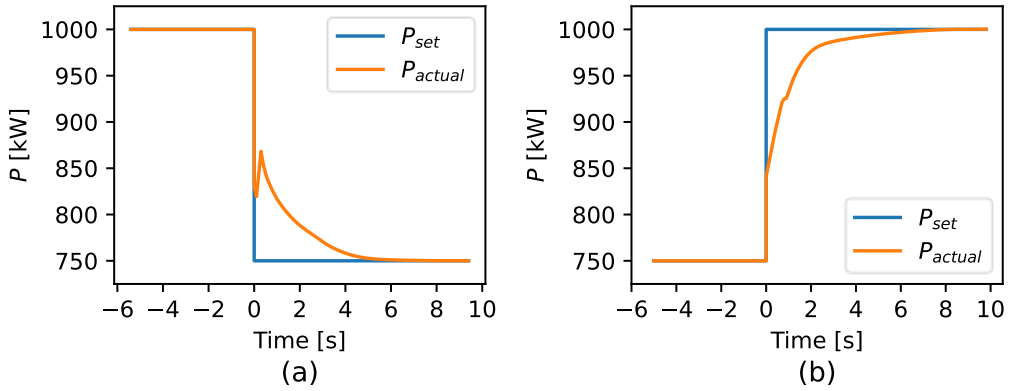

Fig. 2. Response of a 1 MW heat pump to a 250 kW downward (a) and upward (b) step in compressor power.

Next to this suitable response time, it is crucial that the delivery temperature to the TES-system remains correct during the power modulation. In Figure 3, the variation of the water temperature at the outlet of the condenser is shown for the downward and upward step. The maximum absolute deviation is 0.59 °C and 0.66 °C for the downward and upward step, respectively. Besides, the duration of the deviation is lower than 50 s. Despite this short duration, it is still noticeable that the temperature response is significantly slower than the power response.

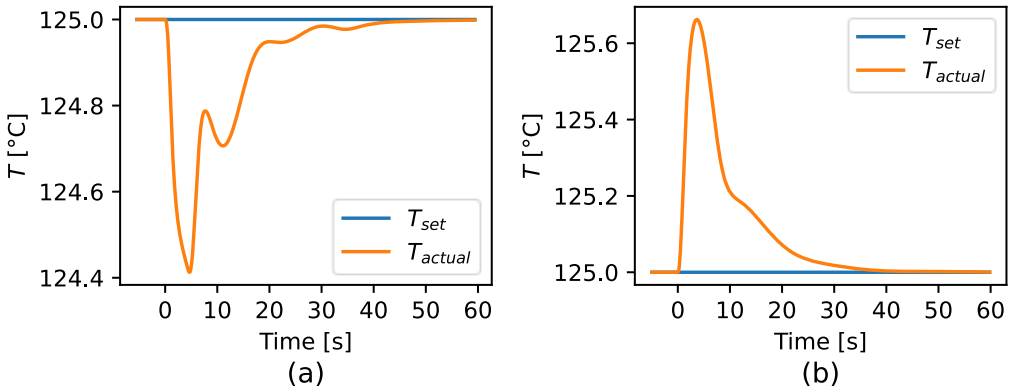

Fig. 3. Water temperature at the outlet of the condenser for a 250 kW downward (a) and upward (b) step in compressor power.

To better understand this delayed thermal response, the system's reaction to a 250 kW downward step in compressor power setpoint (P_{set}) is investigated. The response to the upward step is analogous. In Figure 4, it can be seen that the PI-controller of the compressor reacts immediately on the reduced power setpoint by lowering the compressor speed (n). Consequently, the refrigerant mass flow ($\dot{m}_r$) reduces. Moreover, the evaporator pressure drops and the condenser pressure increases, which results in a reducing pressure ratio (PR) over the compressor. As both changes happen quickly, the compressor power settles rapidly at the desired setpoint. The delayed temperature response of the sink water can be explained by the thermal inertia of the heat exchanger. As visualized in Figure 5, the thermal inertia causes the condenser heat rate ($\dot{Q}_{cond,out}$) to drop slower compared to the refrigerant mass flow and enthalpy of the refrigerant at the compressor outlet. Therefore, the water temperature at the sink outlet drops more slowly as well. As the heat sink PI-controller reacts based on the difference between this temperature and the desired temperature setpoint, its reaction is delayed compared to the compressor PI-controller that reacts directly on the desired electrical power consumption. The sink PI-controller's response is thus cushioned by the inertia of the heat exchanger. Nevertheless, the PI-controller of the sink reacts sufficiently quickly to maintain a suitable water temperature at the condenser outlet.

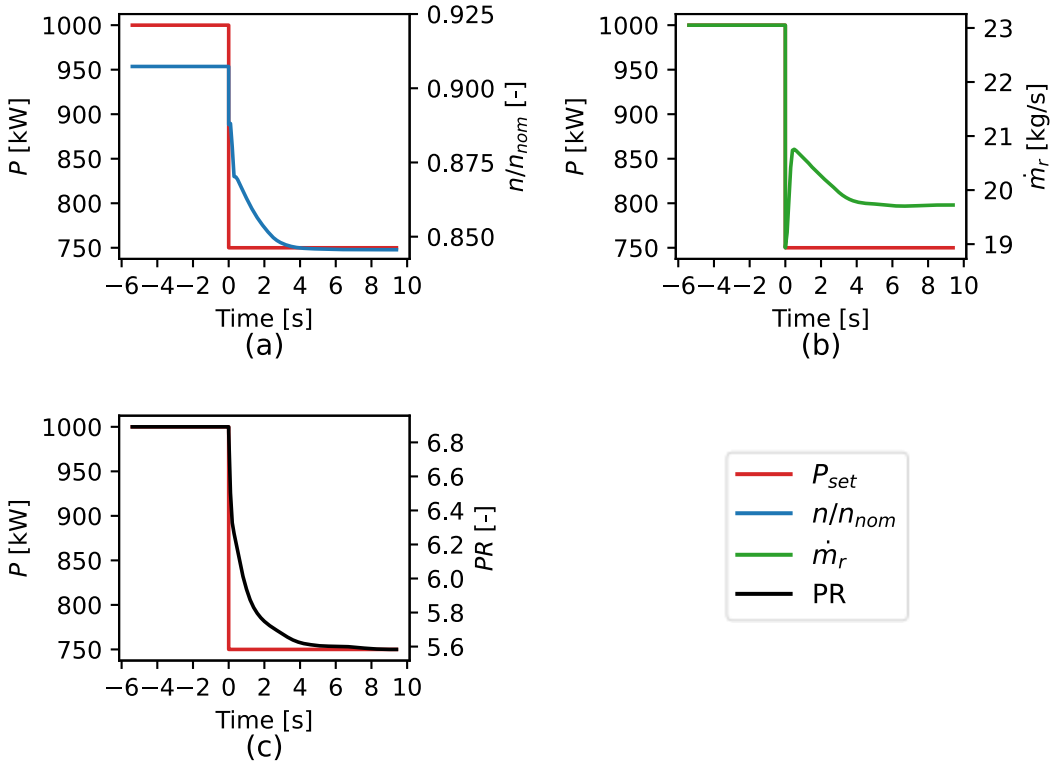

Fig. 4. System response for a 250 kW downward step in compressor power: (a) relative compressor speed, (b) refrigerant mass flow rate, (c) pressure ratio.

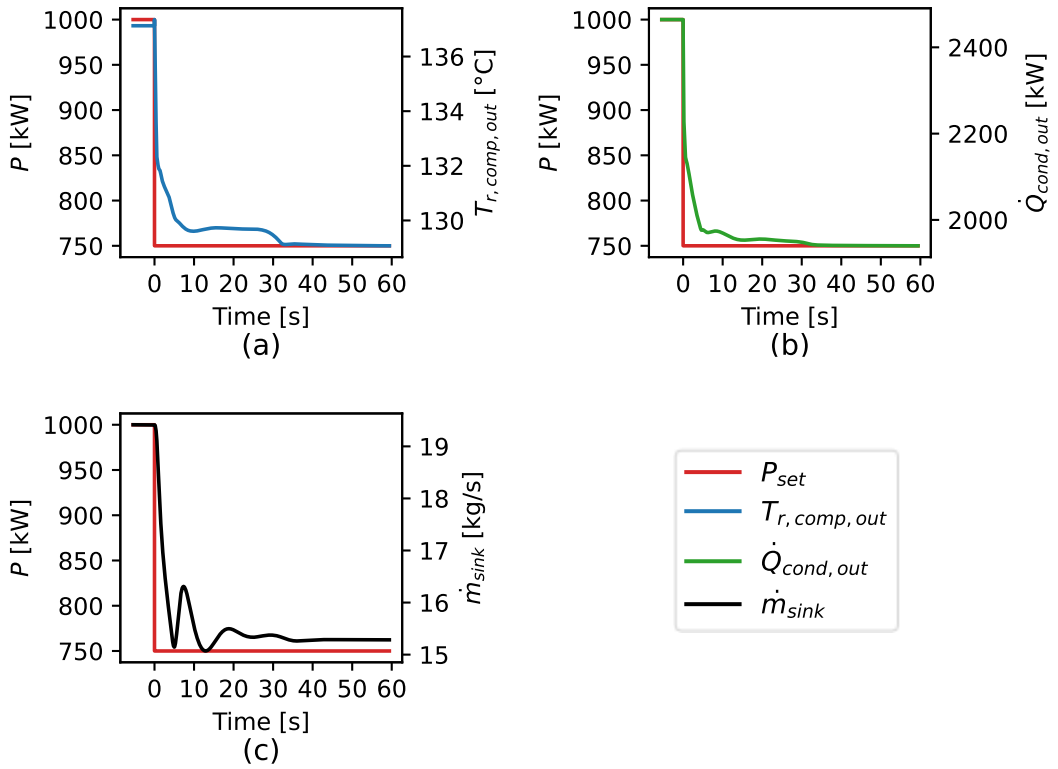

Fig. 5. System response for a 250 kW downward step in compressor power: (a) refrigerant temperature at compressor outlet, (b) condenser heat rate, (c) water mass flow heat sink.

As the FAT is well below the required limit while maintaining adequate supply temperatures to the TES, it can be concluded that the heat pump system is capable of delivering a capacity of 250 kW mFRR in both the upward and downward direction. However, it is important to note that the power control acts directly on the compressor setpoint and that this compressor is modelled assuming quasi-steady state. Given the low FAT found, taking the compressor dynamics into account may thus be important for grid supporting applications in contrast to traditional heat pump applications where the heat pump is controlled based on heat demand. The sensitivity of the system's response to the compressor inertia will be evaluated in future work.

3.4. Secondary reserve

Compared to tertiary reserve, aFRR requires a faster response with a FAT lower than 7.5 min. This limit will be reduced to 5 minutes by 17/12/2024 [12]. As discussed in Section 3.3, the heat pump meets this requirement while maintaining suitable TES-temperatures. Next to the FAT requirement, the heat pump should be able to follow a synthetic load pattern within a margin of 7.5 %. Figure 6 shows this load-pattern for upward and downward aFRR, which corresponds to lowering and increasing the compressor power consumption respectively. A maximum power deviation of 0.85 % and 0.79 % is observed for the upward and downward aFRR product, which is within the allowable limit. The corresponding maximum absolute deviations of the water temperature at the outlet of the condenser are 0.30 °C in both directions. The heat pump thus qualifies for an aFRR capacity of 250 kW in the upward and downward direction.

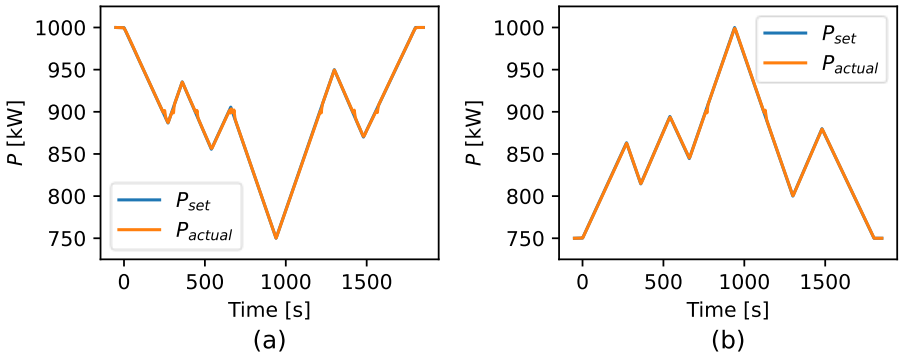

Fig. 6. Load-following test for the (a) upward and (b) downward aFRR product.

3.5. Primary reserve

The qualification test for FCR consists of two parts. First, the FAT of the full contracted reserve should be delivered within 30 s in both directions, a requirement which is met as shown in Table 5. Besides, the system should react adequately to step changes of one fourth of the contracted capacity. The maximum allowable deviation after 12.5 s is 10% of the step (3.125 kW). As explained in Section 3.1, the heat pump is tested for a symmetric capacity of 125 kW. Figure 7 shows the system response on the stepwise decrease and increase of the requested compressor power. The deviation values per step are summarized in Table 6. The maximum absolute deviation of the water temperature at the outlet of the condenser over the whole ramping interval is 0.27 and 0.13 °C for the stepwise decrease and increase in requested compressor power, respectively. The system thus qualifies for a symmetric FCR capacity of 125 kW.

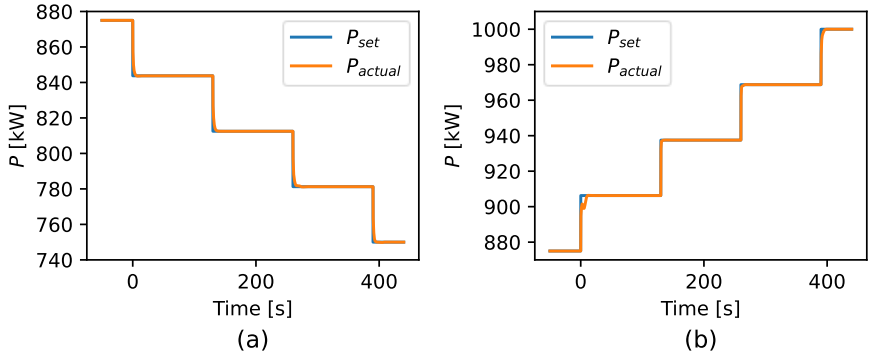

Fig. 7. System's response to stepwise (a) decrease and (b) increase of requested compressor power.

Table 6. Overview of power deviations in FCR qualification test.

	Decrease compressor power		Increase compressor power	
Step	P_{set} [kW]	Largest deviation [kW]	P_{set} [kW]	Largest deviation [kW]
1	843.750	0.0435	906.250	0.0339
2	812.500	0.0397	937.500	0.0100
3	781.250	0.157	968.750	0.009
4	750.00	0.213	1000.00	0.006

4. Conclusion

The possibility to deliver grid balancing services with large-scale heat pumps in Rankine-based Carnot battery systems was investigated. Therefore, a basic Rankine-based 1 MW heat pump cycle, suitable for implementation in a Carnot battery using two-tank liquid storage, was modelled dynamically in Modelica. Afterwards, a suitable system control strategy was developed and the system was evaluated according to the pre-qualification tests for grid balancing services in the European grid. Under the assumption of quasi-steady state compressor modelling and ideal behavior of the sensible storage tanks, the heat pump can deliver a symmetric capacity of 125 kW for FCR while maintaining correct delivery temperatures to the TES. Alternatively, the system can offer a capacity of 250 kW for aFRR and mFRR in both the upward and downward direction. These results indicate that the delivery of grid balancing services could be another revenue stream to increase the financial feasibility of Carnot battery systems and it is thus worthwhile to investigate the potential financial benefits. In future work, the sensitivity of the results to the compressor's inertia will be validated and the dynamic model will be extended to a full dynamic Carnot battery model including detailed modelling of the TES and organic Rankine cycle, hence further investigating optimal system scheduling within the energy system.

References

[1] International Energy Agency, Energy transition indicators, 2020. https://www.iea.org/data-and-statistics/data-browser?country=WORLD&fuel=Energy%20transition%20indicators&indicator=ETISharesInPowerGen (Accessed 30.06.2021.
[2] M.C. Argyrou, P. Christodoulides, S.A. Kalogirou, Energy storage for electricity generation and related processes: Technologies appraisal and grid scale applications, Renewable and Sustainable Energy Reviews 94 (2018) 804-821.
[3] C. Andrey, P. Barberi, L. Lacombe, L. van Nuffel, F. Gérard, J.G. Dedecca, K. Rademaekers, Y. El Idrissi, M. Crenes, Study on energy storage – Contribution to the security of the electricity supply in Europe, European Commission, Luxembourg, 2020.
[4] J.D. McTigue, P. Farres-Antunez, K.S. J, C.N. Markides, A.J. White, Techno-economic analysis of recuperated Joule-Brayton pumped thermal energy storage, Energy Conversion and Management 252 (2022).
[5] O. Dumont, G.F. Frate, A. Pillai, S. Lecompte, M. De paepe, V. Lemort, Carnot battery technology: A state-of-the-art review, Journal of Energy Storage 32 (2020).
[6] R. Tassenoy, K. Couvreur, W. Beyne, M. De Paepe, S. Lecompte, Techno-economic assessment of Carnot batteries for load-shifting of solar PV production of an office building, Renewable Energy 199 (2022) 1133-1144.
[7] A. Vecchi, K. Knobloch, T. Liang, H. Kildahl, A. Sciacovelli, K. Engelbrecht, Y. Li, Y. Ding, Carnot Battery development: A review on system performance, applications and commercial state-of-the-art, Journal of Energy Storage 55 (2022).
[8] T. Heggarty, J.-Y. Bourmaud, R. Girard, G. Kariniotakis, Multi-temporal assessment of power system flexibility requirement, Applied Energy 238 (2019) 1327-1336.
[9] J. Villar, R. Bessa, M. Matos, Flexibility products and markets: Literature review, Electric Power Systems Research 154 (2018) 329-340.
[10] elia, Keeping the Balance, 2022. https://www.elia.be/en/electricity-market-and-system/system-services/keeping-the-balance. (Accessed 06/11/2022.
[11] elia, FCR service design note, 2019.
[12] elia, Automatic Frequency Restoration Process (aFRR/R2), 2022. https://www.elia.be/en/electricity-market-and-system/system-services/keeping-the-balance/afrr. (Accessed 06/11/2022.

[13] elia, Balancing services: mFRR - design note, 2022.
[14] C. Lu, X. Shi, Q. He, Y. Liu, X. An, S. Cui, D. Du, Dynamic modeling and numerical investigation of novel pumped thermal electricity storage system during startup process, Journal of Energy Storage 55 (2022).
[15] H. Yang, J. Li, Z. Ge, L. Yang, X. Du, Dynamic characteristics and control strategy of pumped thermal electricity storage with reversible Brayton cycle, Renewable Energy 198 (2022) 1341-1353.
[16] A. David, B.V. Mathiesen, H. Averfalk, S. Werner, H. Lund, Heat Roadmap Europe: Large-Scale Electric Heat Pumps in District Heating Systems, Energies 10(4) (2017).
[17] W. Meesenburg, W.B. Markussen, T. Ommen, B. Elmegaard, Optimizing control of two-stage ammonia heat pump for fast regulation of power uptake, Applied Energy 271 (2020).
[18] G.F. Frate, M. Antonelli, U. Desideri, A novel Pumped Thermal Electricity Storage (PTES) system with thermal integration, Applied Thermal Engineering 121 (2017) 1051-1058.
[19] A. Marina, S. Spoelstra, H.A. Zondag, A.K. Wemmers, An estimation of the European industrial heat pump market potential, Renewable and Sustainable Energy Reviews 139 (2021).
[20] G.F. Frate, L. Ferrari, U. Desideri, Multi-Criteria Economic Analysis of a Pumped Thermal Electricity Storage (PTES) With Thermal Integration, Frontiers in Energy Research 8 (2020).
[21] A. Rahman, A.D. Smith, N. Fumo, Performance modeling and parametric study of a stratified water thermal storage tank, Applied Thermal Engineering 100 (2016) 668-679.
[22] C. Arpagaus, F. Bless, M. Uhlmann, J. Schiffmann, S.S. Bertsch, High temperature heat pumps: Market overview, state of the art, research status, refrigerants, and application potentials, Energy 152 (2018) 985-1010.
[23] A.H.H. Jose M Corberan, Jorge Paya, Thermodynamic analysis and selection of refrigerants for high temperature heat pumps, in: I.E.S. Vasile Minea (Ed.) 25th IIR International Congress of Refrigeration, International Institute of Refrigeration IIR, Montréal, Canada, 2019.
[24] G. Kosmadakis, C. Arpagaus, P. Neofytou, S. Bertsch, Techno-economic analysis of high-temperature heat pumps with low-global warming potential refrigerants for upgrading waste heat up to 150 °C, Energy Conversion and Management 226 (2020).
[25] G.F. Frate, L. Ferrari, U. Desideri, Analysis of suitability ranges of high temperature heat pump working fluids, Applied Thermal Engineering 150 (2019) 628-640.
[26] B. Eppinger, L. Zigan, J. Karl, S. Will, Pumped thermal energy storage with heat pump-ORC-systems: Comparison of latent and sensible thermal storages for various fluids, Applied Energy 280 (2020).
[27] S. Quoilin, Next Generation Heat Pumps, 2020.
[28] I.H.B. Eric W. Lemmon, Marcia L. Huber, Mark O. McLinden, REFPROP Documentation, Release 10.0, 2018.
[29] T.M. Association, 2022. https://modelica.org/. (Accessed 06/11/2022.
[30] D.S. AB, Dymola - Dynamic Modelling Laboratory - Full User Manual, 2021.
[31] TLK Thermo GmbH & IfT TIL 3.7 – Model library for thermal components and systems, 2020.
[32] M. Imran, R. Pili, M. Usman, F. Haglind, Dynamic modeling and control strategies of organic Rankine cycle systems: Methods and challenges, Applied Energy 276 (2020).
[33] Funke, PLATE HEAT EXCHANGERS - Variety and top product quality, 2022. 26/04/2022).
[34] Swep, Plate Heat Exchangers - products, 2022. https://www.swep.net/products/.
[35] J.D. Craecker, Performance analysis of heat pumps in Carnot battery systems for grid balancing services, in: G. University (Ed.) 2022, p. 90.
[36] J.G. Collier, Thome, J.R., Convective Boiling and Condensation, 3rd ed.1996.
[37] H.D. Baehr, Stephan, K., Wärme- und Stoffübertragung, 2 ed.1996.
[38] M. Holger, Pressure Drop and Heat Transfer in Plate Heat Exchangers, 2010.
[39] K. Hoopes, T.C. Allison, R. Kurz, Oil and Gas Compressor Basics, Compression Machinery for Oil and Gas2019, pp. 3-11.
[40] GasTurb, GasTurb 14 - free trail, 2022.
[41] R. Pili, A. Romagnoli, M. Jiménez-Arreola, H. Spliethoff, C. Wieland, Simulation of Organic Rankine Cycle – Quasi-steady state vs dynamic approach for optimal economic performance, Energy 167 (2019) 619-640.
[42] W.K. Meesenburg, René; Ommen, Torben; Markussen, Wiebke Brix; Elmegaard, Brian, Design considerations for dynamically operated large-scale ammonia heat pumps, 25th IIR International Congress of Refrigeration, International Institute of Refrigeration, Montréal, Canada, 2019.
[43] pidtuner, pidtuner - tune your PID, 2022. https://pidtuner.com/#/.